Journal of Alloys and Compounds 509 (2011) 9733–9741

Contents lists available at ScienceDirect

Journal of Alloys and Compounds

journal homepage: www.elsevier.com/locate/jallcom

First-principles study of lattice dynamics and thermodynamic properties of $LiInX_2$ (X = S, Se, Te)

Tianhui Ma[a,b,*], Liang Sun[c], Chao Xu[b], Yufeng Chen[a]

[a] College of Chemistry and Chemical Engineering, Mudanjiang Normal University, Mudanjiang 157012, China
[b] School of Chemical Engineering and Technology, Harbin Institute of Technology, Harbin 150001, China
[c] School of Physics and Electronic Engineering, Yibin University, Yibin 644000, China

ARTICLE INFO

Article history:
Received 2 July 2011
Received in revised form 30 July 2011
Accepted 1 August 2011
Available online 10 August 2011

Keywords:
Orthorhombic lattice
Chalcopyrite
Lattice dynamics
Thermodynamic properties

ABSTRACT

First-principles calculations of lattice dynamics and thermodynamic properties of orthorhombic $LiInS_2$ and $LiInSe_2$ and chalcopyrite $LiInTe_2$ have been performed within density functional perturbation theory using norm conserving pseudopotentials. Theoretical values of phonon mode frequencies are in good agreement with the experimental data available for these crystals obtained by methods of Raman spectroscopy and infrared one. In the whole frequency range a significant decrease of the vibrational frequencies is observed going from $LiInS_2$ to $LiInSe_2$ and $LiInTe_2$, which is a consequence of the anion radius increase. The lattice vibrations of In–X (X = S, Se, Te) bonds are mainly located in the low-frequency and mid-frequency ranges, and the Li–X bond vibrations are dominated in the higher frequency range. The mixed covalent–ionic nature of the three compounds is manifested by Born effective charge data. The vibration patterns of orthorhombic $LiInS_2$ and chalcopyrite $LiInTe_2$ were discussed in detail. The temperature dependences of thermodynamic quantities (including the internal energy, free energy, heat capacity, entropy and the Debye temperature Θ_D) of all the three compounds were also presented in this paper. It is proved that Debye stiffness increases from $LiInTe_2$ to $LiInSe_2$ and $LiInS_2$.

1. Introduction

Ternary lithium compounds $LiInX_2$ (X = S, Se, Te), which are considered as promising materials for nonlinear optical applications in the mid-IR, have recently attracted a lot of attention due to their unique optical properties: a wide transparency range; a sufficiently large birefringence; good thermo-mechanical properties and a small two-photon absorption coefficient [1–6]. The light Li^+ ions can not only enlarge the band gaps of these compounds and further lead to a high laser induced damage thresholds (LIDT), but also increase the frequencies of crystal lattice vibrations and the Debye temperature. The outstanding advantage in growth for orthorhombic $LiInS_2$ and $LiInSe_2$ is the weak tendency to stresses and laminar defects due to no obvious anisotropy in the thermal expansion coefficients [4]. The properties of $LiInS_2$ and $LiInSe_2$ semiconductors have been investigated in experiments by Isaenko et al., which exhibit the better nonlinearity and figure of merit for nonlinear optical applications on optical parametric oscillator (OPO) and second harmonic generation (SHG) in the mid-IR [4–6]. The pyroelectricity, thermal conductivity, thermal expansion, and thermo-optic coefficients of $LiInS_2$ and $LiInSe_2$ were also measured by Yelisseyev et al. [1,7]. Though the large-size $LiInTe_2$ crystals with high optical quality have not been successfully grown, the analog compound $LiGaTe_2$ has been demonstrated to be a promising material for OPO and SHG devices in the mid-IR [8,9]. In theory, the structural, electronic and optical properties of $LiInS_2$ and $LiInSe_2$ have been in detail studied [10,11]. It was indicated that a strong hybridization between In – 5*s*, 5*p* orbits and S – 3*p* (Se – 4*p*) orbits at upper valence bands is the important structural characteristics of these compounds [10]. Basalaev et al. studied the chemical bonding and electronic structure of chalcopyrite $LiInSe_2$ and $LiInTe_2$, indicating a donor–acceptor bond peculiarity [12]. Li et al. demonstrated that Li cations in $LiBX_2$ (B = Al, Ga and In; X = S, Se, Te) compounds play an important role in the stabilization of the structures by comparing the electronic structures of $Li_4Al_4Se_8$ and Al_4Se_8 [13]. Li et al. investigated the structure, electronic properties, optical properties, lattice dynamics and thermodynamic properties of $LiInSe_2$ polymorph (β-$NaFeO_2$-type, α-$NaFeO_2$-type and $CuFeS_2$-type), indicating that the α-$NaFeO_2$-type $LiInSe_2$ has the broader density of states, smaller band gap and special optical properties [11]. The lattice dynamics and elastic constants of $LiBTe_2$ (B = Al, Ga, In) compounds were analyzed and compared with the Cu- and Ag-based analogs [14]. The dielectric spectra, birefringence and second harmonic generation of $AGaX_2$ (A = Ag and Cu) semiconductors

* Corresponding author at: College of Chemistry and Chemical Engineering, Mudanjiang Normal University, Mudanjiang 157012, China. Tel.: +86 451 86221281; fax: +86 451 86221281.
E-mail address: matianhui1972921@163.com (T. Ma).

0925-8388/$ – see front matter © 2011 Elsevier B.V. All rights reserved.
doi:10.1016/j.jallcom.2011.08.006

being the birefringent non-linear mid-IR optical crystals have been experimentally and theoretically investigated [15,16]. The bond characteristics in the Li-containing compounds are different from that of Cu- and Ag-based analogs. Li is merely an electron donator and hardly contributes to the frontier orbitals because of the small ion radius and simple extra nuclear electron configuration, which leads to the unique optical properties of Li-containing compounds. So, the further theoretical investigations concerning the microscopic properties are very necessary for their applications.

In this paper, the lattice vibrations, Raman spectra, infrared absorption spectra and thermodynamic properties of $LiInS_2$, $LiInSe_2$ and $LiInTe_2$ have been in detail studied within density functional perturbation theory (DFPT) using norm-conserving pseudopotentials (NCP) and a plane-wave basis set. Our investigations provide useful information for the potential applications of these materials. The wide variety of physical properties of crystals at finite temperatures depends on their lattice dynamical behaviors. So, it is important to understand the vibrational properties and the resulting thermodynamic properties of the crystals. It may be difficult to treat properly all obtained frequencies in experiments, e.g. to detect the presence of vibrations in Raman spectra forbidden by the selection rules, while accurate theoretical calculations can simplify the experimental process and help to interpret the experimental data truly. The thermodynamic properties of $LiInS_2$ and $LiInTe_2$, such as the heat capacity and Debye temperature, which are important parameters for the measurement of crystal physical properties, are firstly given in this paper. The different anions in $LiInS_2$, $LiInSe_2$ and $LiInTe_2$ compounds not only change the unit-cell structures from the orthorhombic structure to the chalcopyrite one, but also affect their various properties. From a fundamental point of view, it would be very important for the applications to study $LiInX_2$ (X = S, Se, Te) as a model ternary chalcogenide to understand how the lattice dynamics and thermodynamic properties are controlled by their compositions and structures.

2. Method of calculations

Calculations of dynamical properties were performed by the use of the linear response method within DFPT [17] as implemented in the Castep package [18]. Dynamic characteristics are rather sensitive to evaluate accurately electronic properties – total energy, electronic density and its derivatives. In the present paper all calculations have been carried out using NCP [19] with a plane wave cutoff energy of 500 eV. The related electronic configurations are In: $5s^2\ 5p^1$, S: $3s^2\ 3p^4$, Se: $4s^2\ 4p^4$, Te: $5s^2\ 5p^4$ and Li: $2s^1$. The k-point meshes for Brillouin zone sampling were constructed using the Monkhorst–Pack scheme and the k-point meshes of $4 \times 3 \times 4$ and $4 \times 4 \times 2$ were used in $LiInX_2$ (X = S, Se) and $LiInTe_2$ systems, respectively. The exchange-correlation effects are found to be significant for the theoretical dynamical properties, especially in the cases of $LiInS_2$ and $LiInSe_2$. The tests on the IR absorption spectra with respect to the exchange-correlation energy have been made. The local density approximation (LDA) by adding the Perdew–Zunger [20] exchange term to the Ceperley–Alder [21] correlation energy was used for $LiInS_2$, while the generalized gradient approximation (GGA) approach was taken into account for $LiInSe_2$ and $LiInTe_2$ by adding the Perdew–Wang (PW91) [22] exchange-correlation terms.

Table 1
Optimized structural parameters (Å) and experimental data (Å) of $LiInS_2$, $LiInSe_2$ and $LiInTe_2$.

Compound		a	b	c
$LiInS_2$	Calculation	6.650	7.843	6.298
	Experiment[a]	6.823	8.266	6.524
$LiInSe_2$	Calculation	7.085	8.251	6.751
	Experiment[a]	7.183	8.398	6.781
$LiInTe_2$	Calculation	6.349	6.349	12.342
	Experiment[a]	6.398	6.398	12.460

[a] Data taken from Ref. [5].

The calculations were assured a very high level convergence with respect to all parameters: the total-energy difference within 1.0×10^{-6} eV/atom, the maximum Hellmann–Feynaman force within 0.01 eV/Å, the maximum stress within 0.02 GPa and the maximum atom displacement within 1.0×10^{-4} Å.

Based on the theory of the quantum statistics within the quasi-harmonic approximation, the calculated value of the total phonon density of states (DOS) was used to evaluate the temperature dependence of the thermodynamic quantities. The entropy of a system has two terms, i.e. the configurational and vibrational entropies. Only the vibrational entropy needs to be considered for the crystalline system without a phase transition. The temperature dependences of the vibrational entropy S, the constant-volume heat capacity C_V and the constant-volume heat capacity in the Debye model C_V^D are given by [17,23]:

$$S(T) = k_B \left\{ \int_0^\infty \frac{\hbar\omega/k_BT}{\exp(\hbar\omega/k_BT)-1} F(\omega)d\omega - \int_0^\infty F(\omega) \ln\left[1-\exp\left(-\frac{\hbar\omega}{k_BT}\right)\right] d\omega \right\} \quad (1)$$

$$C_V(T) = k_B \int_0^\infty \frac{(\hbar\omega/k_BT)^2 \exp(\hbar\omega/k_BT)}{[\exp(\hbar\omega/k_BT)-1]^2} F(\omega)d\omega \quad (2)$$

$$C_V^D(T) = 9Nk_B \left(\frac{T}{\Theta_D}\right)^3 \int_0^{\Theta_D/T} \frac{x^4 e^x}{(e^x-1)^2} dx \quad (3)$$

where k_B is the Boltzmann constant, $\hbar$ is Planck's constant, $F(\omega)$ is the phonon DOS, N is the number of atoms per cell, and Θ_D is the Debye temperature at a given temperature T. By fitting the theoretical C_V^D, the temperature dependence of Θ_D can be obtained.

3. Results and discussion

3.1. Structural properties

$LiInS_2$ and $LiInSe_2$ are the orthorhombic β-$NaFeO_2$-type structure (space group $Pna2_1$, point group $mm2$), which presents a distorted superstructure of the wurtzite lattice, whereas $LiInTe_2$ is the chalcopyrite $CuFeS_2$-type structure (space group $I\bar{4}2d$, point group $\bar{4}2m$) [5]. The chalcopyrite structure is closely related to the sphalerite or zinc-blende structure and can be considered as a result of the regular substitution of the sphalerite cations by atoms of I and III groups. The orthorhombic and chalcopyrite structures are both characterized by a closest anion packing according to the ratio

Table 2
Born effective charges Z^* in atomic units, X denotes S, Se and Te, respectively.

	$LiInS_2$	$LiInSe_2$	$LiInTe_2$
Z^*_{Li}	$\begin{pmatrix} 0.96 & 0.05 & 0.07 \\ -0.12 & 1.04 & -0.09 \\ -0.04 & 0.10 & 1.02 \end{pmatrix}$	$\begin{pmatrix} 1.00 & -0.05 & 0.08 \\ 0.15 & 1.09 & 0.12 \\ -0.05 & -0.11 & 1.07 \end{pmatrix}$	$\begin{pmatrix} 1.09 & -0.17 & 0.00 \\ 0.17 & 1.09 & 0.00 \\ 0.00 & 0.00 & 0.88 \end{pmatrix}$
Z^*_{In}	$\begin{pmatrix} 2.64 & -0.19 & -0.14 \\ 0.34 & 2.49 & 0.27 \\ 0.09 & -0.33 & 2.72 \end{pmatrix}$	$\begin{pmatrix} 2.57 & 0.22 & -0.17 \\ -0.40 & 2.41 & -0.34 \\ 0.10 & 0.37 & 2.65 \end{pmatrix}$	$\begin{pmatrix} 2.35 & 0.48 & 0.00 \\ -0.48 & 2.35 & 0.00 \\ 0.00 & 0.00 & 2.67 \end{pmatrix}$
$Z^*_{X_1}$	$\begin{pmatrix} -1.47 & -0.23 & -0.11 \\ -0.07 & -1.77 & -0.28 \\ -0.11 & -0.29 & -2.15 \end{pmatrix}$	$\begin{pmatrix} -1.46 & -0.20 & -0.10 \\ -0.04 & -1.77 & -0.29 \\ -0.11 & -0.28 & -2.13 \end{pmatrix}$	$\begin{pmatrix} -1.58 & 0.00 & 0.00 \\ 0.00 & -1.87 & 0.28 \\ 0.00 & 0.34 & -1.78 \end{pmatrix}$
$Z^*_{X_2}$	$\begin{pmatrix} -2.12 & -0.35 & 0.01 \\ -0.26 & -1.75 & -0.10 \\ 0.06 & -0.11 & -1.59 \end{pmatrix}$	$\begin{pmatrix} -2.16 & -0.33 & -0.01 \\ -0.24 & -1.73 & 0.09 \\ -0.06 & 0.09 & -1.59 \end{pmatrix}$	$\begin{pmatrix} -1.87 & 0.00 & -0.28 \\ 0.00 & -1.58 & 0.00 \\ -0.34 & 0.00 & -1.78 \end{pmatrix}$

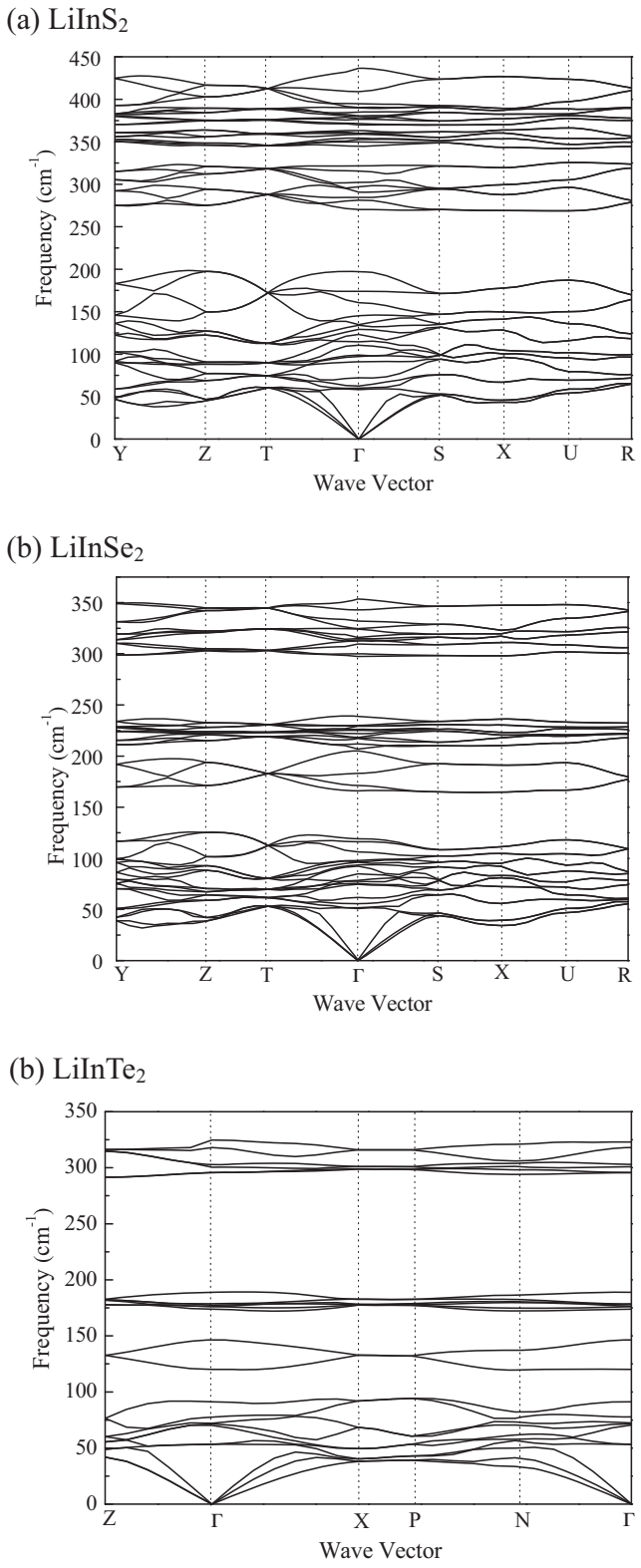

Fig. 1. Calculated phonon dispersion spectra of: (a) $LiInS_2$, (b) $LiInSe_2$ and (c) $LiInTe_2$.

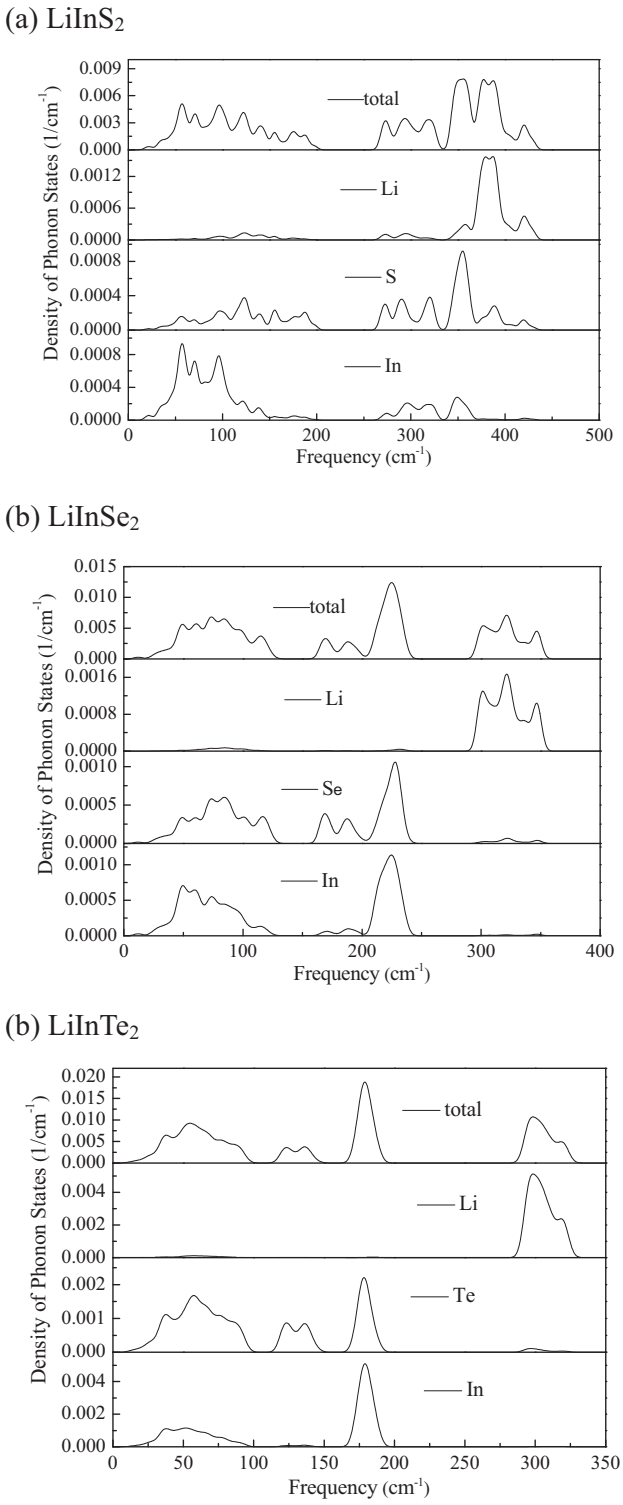

Fig. 2. Total and partial phonon density of states of: (a) $LiInS_2$, (b) $LiInSe_2$ and (c) $LiInTe_2$.

$\frac{4}{3}N\pi R^3/V = 0.74$, where R is the anion radius, N is the number of chalcogen atoms per cell and V is the cell volume [5]. So, the main characteristics of the two structures are that each cation (Li and In) is surrounded by four atoms of anion, and each anion is surrounded by two Li and two In atoms. The difference of the two structures is caused by the different way of the anion packing. The orthorhombic structure is closest to hexagonal packing of the anions, while the chalcopyrite structure is closest to anion face-centered cubic packing.

The experimental lattice parameters [5] were used as a starting point for geometry optimization. The experimental and optimized lattice parameters are listed in Table 1. The optimized lattice parameters are slightly smaller than the experimental values according to our methods, while the maximal deviations with respect to experimental values are within the normal agreement

Table 3
Static ε_0, high frequency ε_∞ and lattice ε^{lat} dielectric constants of $LiInS_2$, $LiInSe_2$ and $LiInTe_2$.

Compound	ε_∞	ε_0	ε^{lat}	Experiment
$LiInS_2$	4.641	7.020	2.379	–
$LiInSe_2$	4.851	7.300	2.449	ε_0 = 7.59[b]
$LiInTe_2$	6.103	8.209	2.106	ε_∞ = 6.29[c]
	7.297[a]			ε_0 = 7.89[c]

[a] Data taken from Ref. [14].
[b] Data taken from Ref. [25].
[c] Data taken from Ref. [26].

by LDA and GGA standards, which is sufficient to allow the further study of dynamical and thermodynamic properties.

3.2. Lattice dynamics

The primitive unit cell of orthorhombic $LiInS_2$ and $LiInSe_2$ contains sixteen atoms with 48 normal modes at the center of the Brillouin zone, which can be described by the irreducible representations of the point group C_{2V} as follows:

$$\Gamma_O = 12A_1 + 12A_2 + 12B_1 + 12B_2 \quad (4)$$

where the acoustic modes are A_1, B_1 and B_2. The remaining 45 optical modes contain 33 infrared active vibration modes ($11A_1 + 11B_1 + 11B_2$) and 12 Raman active modes ($12A_2$). The long-range behavior of the coulomb interaction gives rise to macroscopic electric field for longitudinal optical (LO) phonons and transverse optical (TO) ones, and the coupling between the phonon modes and the electric field leads to the LO–TO splitting at the Γ point. The difference between LO and TO phonon frequencies is defined by the tensor of Born effective charges Z^* and high-frequency dielectric tensor ε_∞ through nonanalytic contribution to the force constants. All these quantities are calculated in terms of the DFPT and no addi-

Table 4
Phonon frequencies (cm^{-1}) of $LiInS_2$, $LiInSe_2$ and $LiInTe_2$ at Γ point.

$LiInS_2$		$LiInSe_2$		$LiInTe_2$	
Symmetry	Raman	Symmetry	Raman	Symmetry	Raman
A_2	60.02	A_2	51.77	B_1	77.91
A_2	72.33	A_2	61.86	A_1	120.12
A_2	123.24	A_2	84.76	B_1	173.73
A_2	129.22	A_2	96.65	B_1	317.98
A_2	160.59	A_2	106.22		IR
A_2	270.27	A_2	171.29	E(TO)	53.26
A_2	315.76	A_2	217.10	B_2	70.23
A_2	349.94	A_2	226.23	E(LO)	71.53
A_2	359.96	A_2	229.18	E(TO)	176.21
A_2	371.19	A_2	299.88	B_2(TO)	176.24
A_2	379.74	A_2	313.47	E(LO)	178.73
A_2	409.16	A_2	342.81	E(TO)	295.56
	IR		IR	B_2(LO)	300.47
A_1	58.45	A_1	50.86	E(LO)	303.05
B_2	62.50	B_2	55.69		Silent
A_1	90.92	B_2	74.76	A_2	91.32
B_2	97.17	A_1	75.57	A_2	146.53
B_1	98.96	A_1	77.61		
B_1	110.46	B_1	78.35		
A_1	114.73	B_2	91.34		
B_2	131.45	B_1	92.504		
A_1	134.10	A_1	96.21		
B_1	144.57	B_1	97.48		
B_2	173.36	B_2	115.95		
B_1	197.45	B_1	119.08		
B_2	281.05	A_1	166.06		
A_1	284.71	B_2	182.74		
A_1	290.60	B_1	204.99		
B_1	294.70	A_1	206.85		
B_1	301.80	B_1	211.33		
B_2	321.30	B_1	216.62		
A_1 (TO)	344.70	B_2	218.30		
B_2 (TO)	348.74	A_1 (TO)	222.10		
A_1 (LO)	353.92	B_2	223.58		
B_1	354.91	B_1 (TO)	225.34		
B_2 (LO)	359.14	A_1 (LO)	229.63		
B_1 (TO)	361.26	B_2	230.25		
A_1	369.93	A_1	297.25		
B_1 (LO)	375.61	B_1 (TO)	307.22		
A_1 (TO)	376.58	B_1 (LO)	312.05		
B_2	379.77	B_2	312.76		
B_1 (TO)	382.48	A_1 (TO)	314.79		
B_2	387.30	B_2 (TO)	320.37		
A_1 (LO)	390.38	A_1 (LO)	324.48		
B_2	392.43	B_2 (LO)	326.70		
B_1 (LO)	395.09	B_1 (LO)	333.46		

tional experimental data are required. Since $LiInS_2$ and $LiInSe_2$ has a mixed ionic–covalent nature of chemical bonding [10], the macroscopic electric field splits the infrared active modes A_1, B_1, and B_2 to transverse A_1 (TO), B_1 (TO), B_2 (TO), and longitudinal A_1 (LO), B_1 (LO), and B_2 (LO) components. The primitive unit cell of the chalcopyrite $LiInTe_2$ contains eight atoms with 24 degrees of freedom. According to the group theory, there are 21 normal modes at the center of the Brillouin zone, and they can be described by the irreducible representations of the point group D_{2d}:

$$\Gamma_O = A_1 + 2A_2 + 3B_1 + 3B_2 + 6E \quad (5)$$

where B_2 and E are polar Raman active modes with TO and LO phonon frequencies, A_1 and B_1 are nonpolar Raman active modes, A_2 is an optically inactive mode, and E and B_2 are also infrared active vibration modes.

The results of Z^* tensors are presented in Table 2 for three nonequivalent atoms. The effective charges for the other atoms can be obtained from those shown in the table by symmetry considerations. The diagonal tensor elements of three nonequivalent atoms for orthorhombic structure are different, whereas the diagonal tensor components of cations satisfy the relation $Z^*_{xx} = Z^*_{yy} \neq Z^*_{zz}$ for chalcopyrite. Because of the internal distortion, anions do not have equivalent effective charge tensors. As seen from the data presented, Z^* diagonal components of three compounds are different from the expected values of ionic charges Li(1+), In(3+), X(2−) from chemical point of view. The difference of Z^* value from the reference static nominal value is an indication of bond polarity. Ghosez et al. reported that the presence of anomalous Z^* requires a modification of the interactions between the occupied and unoccupied electronic states [24]. The discrepancy between Z^* and static nominal value in the three compounds may be interpreted in terms of a mixed covalent–ionic nature of Li–X and In–X bonds. Z^* value of Li atoms are closer to ionic charges Li (+1) as compared with those of the other atoms. So, it can be concluded that the ionic nature of Li–X bonds are stronger than that of In–X bonds.

The average of electronic (ε_∞) and static (ε_0) dielectric constants obtained from the expression ε_∞ (or ε_0) $= (\varepsilon^{xx}_\infty + \varepsilon^{yy}_\infty + \varepsilon^{zz}_\infty)/3$ is shown in Table 3. Our results are in good agreement with the experimental data [25,26]. The static dielectric tensor can be decomposed into the contributions of different modes as follows [27]:

$$\varepsilon_0 = \varepsilon_\infty + \frac{4\pi e^2}{V} \sum_\lambda \frac{S_m}{\omega^2_\lambda} \quad (6)$$

where S_m and ω_λ are the oscillator strength tensor which is related to eigen displacements and Born effective charge tensors and frequency of λ, respectively, $\varepsilon_0 - \varepsilon_\infty$ is the lattice dielectric constant ε^{lat}. Since the mode contribution to the static dielectric constant is inversely proportional to the square of the mode frequency, low frequency modes contribute to ε_0 considerably, although their oscillator strengths are smaller as compared with higher frequency modes. On going from S-containing compound to the Te-containing one there occurs an obvious increase of ε_0 and ε_∞, which is in agreement with the order of electric susceptibility of anions. However, ε^{lat} of the three compounds are similar in our results.

The phonon dispersion curves of three compounds are displayed in Fig. 1 along several high-symmetry lines, and the total and partial phonon DOS are shown in Fig. 2. As follows from the calculations made, the calculated phonon dispersion relations have no soft mode at any wave vectors indicating their stabilities. The closeness between the frequencies of some optic modes and acoustic modes means that energy transfer between these modes is easy. According to inharmonic effects, these low-frequency optic modes will strongly scatter the acoustic modes, which carry the beat flow and may lead to low lattice thermal conductivity [11]. The low LO–TO splitting of three compounds is due to the low ionic characteristics of their structures. It should be noted that the tetrahedral coordinated compounds (such as zinc blende and wurtzite) show much more covalent characteristics than the ionic ones [23].

The phonon dispersion curves of $LiInS_2$ and $LiInSe_2$ are similar and different from the one of $LiInTe_2$ due to different structures. Despite the similarity of $LiInS_2$ and $LiInSe_2$, there are also several distinctions in the phonon dispersion curves because of the different strengths of the elastic forces and the degree of the ionicity. The greatest difference is that two upper phonon bands of $LiInS_2$ are very close with the 16.67 cm^{-1} gaps comparing with the 61.07 cm^{-1} gap for $LiInSe_2$. For $LiInS_2$ two middle phonon bands practically merge from 268.67 cm^{-1} to 325.27 cm^{-1}, whereas for $LiInSe_2$ and $LiInTe_2$ they are separated from each other by 1.79 and 27.21 cm^{-1} gap, respectively. From Fig. 2, the total and partial phonon DOS are similar for $LiInSe_2$ and $LiInTe_2$. The contributions of In and X movements dominate at low-frequency and mid-frequency ranges, and those of Li movements lie at high-frequency range since Li is lighter than In and X. The analysis allows us to conclude that the In–X vibrations are dominated in the low-frequency and mid-frequency regions, and the Li–X vibrations are dominated in the high-frequency region. Li atoms almost keep still when the In–Se and In–Te vibrations are dominated, and movements of Li atoms become quite serious when the phonon frequency is above 280 cm^{-1}. This result is also verified by our following vibrational mode analysis. When the mass of the non-metal atoms increases, four phonon bands of three compounds obviously move towards the lower energy scale because the force constants between cations and anions decrease. While for the chalcopyrite $LiMTe_2$ (M = Al, Ga, In), the third bands move fastest and the shift of other phonon bands is little [14]. This phenomenon can be explained by the fact that the vibrations of Al, Ga and In atoms make a predominant contribution to the mid-range phonon bands for $LiMTe_2$ compounds [14], whereas the vibrations of S, Se and Te atoms influence on all four bands by the formations of In–X and Li–X bonds in compounds. The upper phonon bands are mostly caused by vibrations of Li atoms, and their boundary values for $LiInS_2$, $LiInSe_2$ and $LiInTe_2$ are 436.53, 353.57 and 322.80 cm^{-1}, respectively. The boundary values of $LiAlTe_2$, $LiGaTe_2$ and $LiInTe_2$ are similar at 372, 358 and 349 cm^{-1}, respectively [14].

Results of phonon frequencies of the crystals involved at the center of the Brillouin zone taking into account LO–TO splitting are given in Table 4. LO–TO splitting affects only infrared active modes near Γ point, raising the frequencies of LO modes above those of TO modes. Our mode frequencies of $LiInSe_2$ in high-frequency region are lower than the values by Li et al., while the results in low-frequency and mid-frequency regions are similar to the data by Li et al. [11]. The calculated IR absorption spectra and Raman spectra for the $LiInS_2$, $LiInSe_2$ and $LiInTe_2$ as compared with the experimental values [26,28] are shown in Fig. 3. Along with the increase of the anion radius, all lattice vibration modes of IR and Raman spectra move obviously towards the low energy regions because of the decreasing force constants of cations and anions. According to Fig. 3, the gross features of our calculated spectra agree well with the experimental data for three compounds, but the calculated Raman spectra shift towards high energy region in the ranges 250–400 cm^{-1} and 50–125 cm^{-1} for $LiInS_2$ and $LiInSe_2$, respectively, and the calculated IR spectrum in the range of 270–320 cm^{-1} also shift towards the high frequency region for $LiInS_2$. The discrepancies are mainly caused by the underestimated cell parameters, which correspondingly increase the force constants between cations and anions. However, there is an exception in the high frequency of IR spectrum from 280 cm^{-1} to 350 cm^{-1} for $LiInSe_2$, where the calculated spectra move towards the low frequency region. According to our tests of the exchange-correlation energy, it is found that the different exchange-correlation energy affects mainly the high frequency region of IR spectra, and the

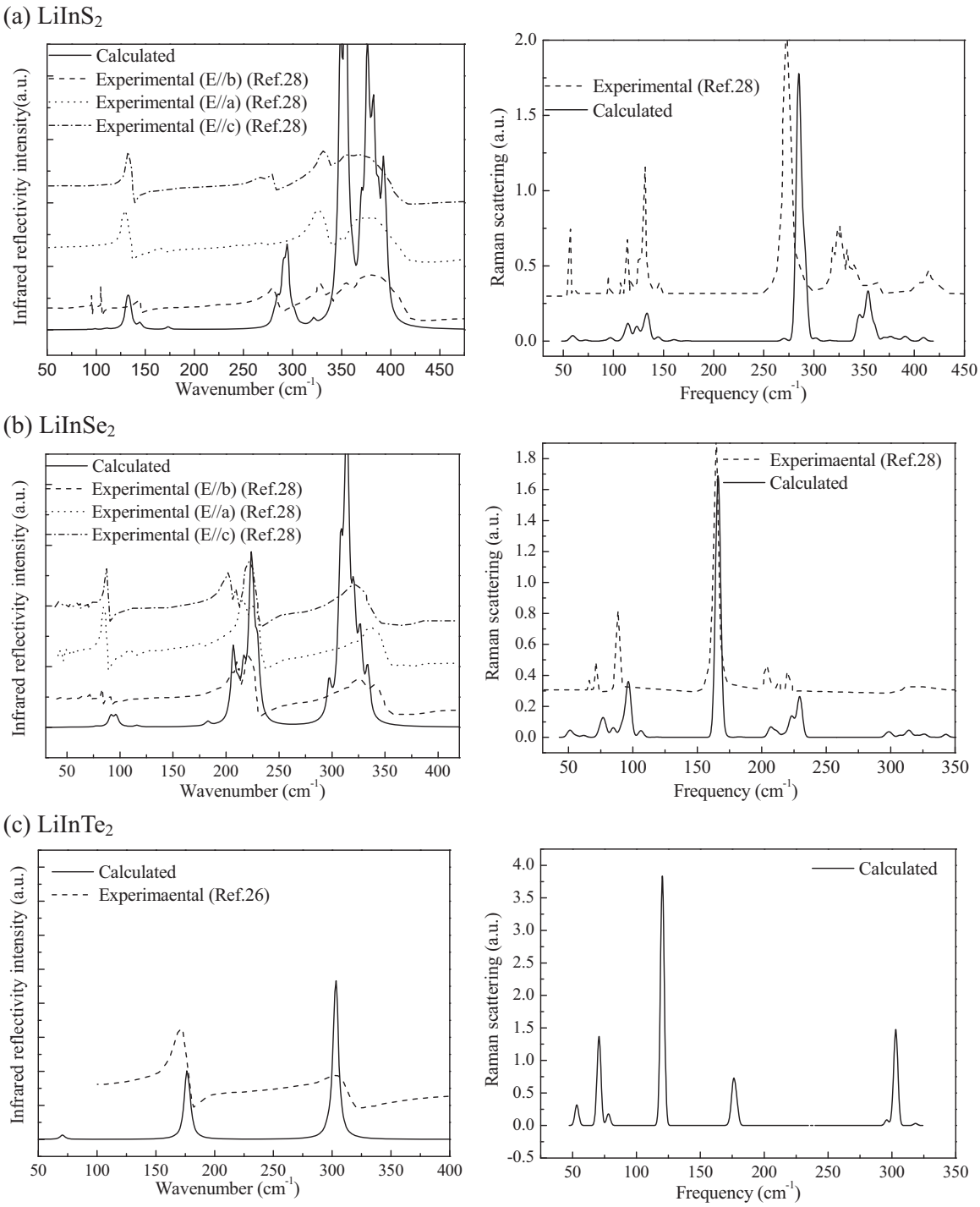

Fig. 3. Calculated infrared reflectivity spectra and Raman spectra compared with the experimental literatures of: (a) $LiInS_2$, (b) $LiInSe_2$ and (c) $LiInTe_2$.

influences on low-frequency and mid-frequency modes are little. Although there is a discrepancy between our data and experimental spectra in this region, our results are closest to the experimental data compared with those by other exchange-correlation energy methods according to our tests. Our results of all modes of $LiInTe_2$ are higher than those in paper [14], the difference was just caused by the different exchange-correlation energy, while our results of IR spectrum are closer to the experimental data. At present, no experimental data of Raman spectra for $LiInTe_2$ are available. Therefore, we consider the present results of $LiInTe_2$ as a predictive study.

Due to low symmetry of orthorhombic structures for $LiInS_2$ and $LiInSe_2$, many peaks appear in the IR and Raman spectra as compared with the tetragonal one, and some peaks are so close to each other that they become one broad peak as shown in Fig. 3. Since there are the analogous vibration modes for $LiInS_2$ and $LiInSe_2$, for simplicity, only vibration patterns of $LiInS_2$ were discussed in detail. In order to have a clear picture of the vibration patterns, we have illustrated the atom displacements for several typical modes as shown in Fig. 4. The vibration motions of low-frequency region ($<110\,cm^{-1}$) are mainly related to the

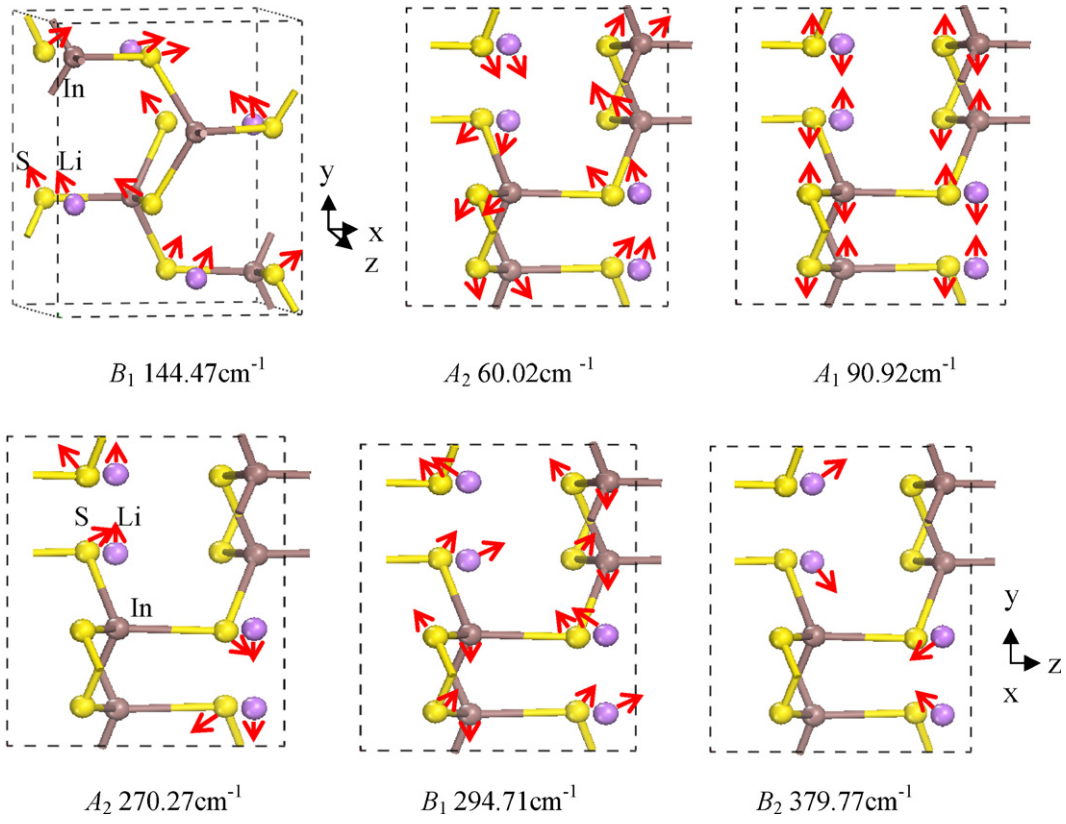

Fig. 4. Atomic displacement patterns of $LiInS_2$.

translational movements of Li, In and S atoms. The vibrations of Raman modes at 60.02 and 72.33 cm^{-1} are along the diagonal axes, while the vibrations of A_1 and B_2 IR modes are along the coordinate axes. There are two B_1 modes at 144.47 and 197.45 cm^{-1} in the 120–200 cm^{-1} regions, which come from the torsion and swing for S–In bonds, and the In atoms are nearly kept still. This is in agreement with the analysis of phonon DOS (see Fig. 2.). The vibration modes at 270.27, 281.06, 284.71, 290.61 and 321.30 cm^{-1} are a combination of stretching and torsion for S–In bonds with Li atoms' translational movements, and the In atoms are almost static for A_2 mode (at 270.27 cm^{-1}). Interestingly only half of S–In bonds in a unit cell take part in the stretching and torsion vibrations, and the other half S–In bonds nearly are still. The B_1 modes at 294.71 and 301.80 cm^{-1} are related to the stretching and torsion movement for all S–In bonds with Li atoms' translational movement. The modes from 344.70 cm^{-1} to 361.27 cm^{-1} are involved in the stretching and torsion movements of S–In bonds with the slight vibrations of In atoms. With the higher vibration frequency, the stretching movements are more obvious. The most intensive peaks of IR spectra at 353.92 and 354.91 cm^{-1} are mainly caused by the symmetry or asymmetry stretching vibrations of half of S–In bonds. For the high-frequency region (>369.94 cm^{-1}), Li atoms have seriously translational motions with each other with slight torsion vibrations of S–In bonds, and the In atoms are still. The higher the vibrational frequency is, the more intensive the translational motions

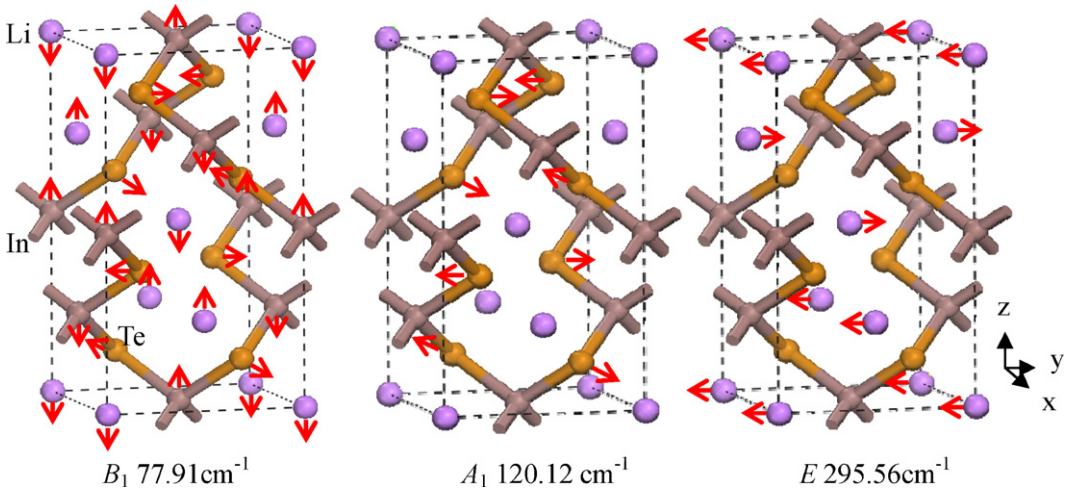

Fig. 5. Atomic displacement patterns of $LiInTe_2$.

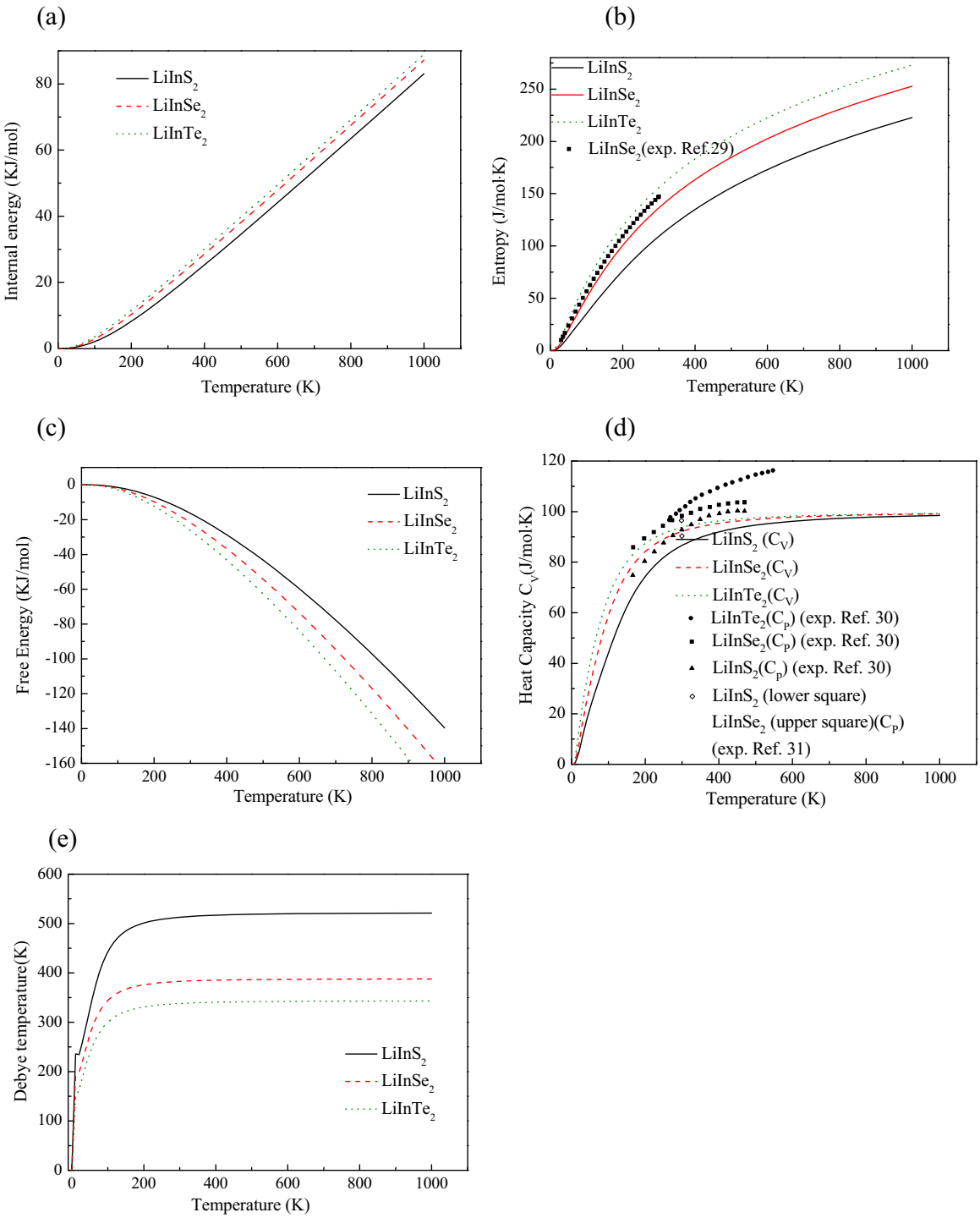

Fig. 6. Calculated temperature dependences of: (a) internal energy, (b) entropy, (c) free energy, (d) constant volume heat capacity and (e) Debye temperature $\Theta_D(T)$ for $LiInS_2$, $LiInSe_2$ and $LiInTe_2$.

of Li atoms are, which is consistent with the results of the phonon DOS.

The atomic displacement patterns for the tetragonal structure $LiInTe_2$ are shown in Fig. 5. The A_1 mode (at 120.12 cm^{-1}) involves the translational movements of Te atoms. One half of Te atoms move against each other along the x axes and the other half of Te atoms move along the y axes, and the Li and In atoms are still. The vibration motions of low-frequency region (<100 cm^{-1}) are mainly related to the swing vibrations of In–Te bonds with the Li and In atoms' translational motions. For the B_1 mode (at 77.91 cm^{-1}) the Li and In atoms have translational motions with each other along z axes, one half of Te atoms move along the y axes, and the other half of Te atoms move along the x axes. The silent mode A_2 at 146.53 cm^{-1} involves the stretching and torsion movements for all Te–In bonds with the In and Li atom still. In the mid-frequency region (170–180 cm^{-1}), the vibration modes are mainly involved in the translational vibrations of In atoms and the torsion movements of Te–In bonds, and the Li atoms are static, which is consistent with the analysis of the phonon DOS. With the higher energy of the vibrations there is the more pronounced effect

in the stretching movements of Te–In bonds. In the high-frequency region (>290 cm^{-1}), the seriously translational vibrations of the Li atoms along the coordination axes or the diagonal axes are main, and the In and Te atoms are still.

3.3. Thermodynamic properties

Fig. 6(a–c) show the calculated thermodynamic quantities (the internal energy, entropy and free energy) of $LiInS_2$, $LiInSe_2$ and $LiInTe_2$ in the temperature range 0–1000 K. The experimental data [29] of $LiInSe_2$ were also given in Fig. 6(b). Although our results are slightly smaller than the experimental ones, theory and experiment show satisfactory agreement within the limitation of the Castep program and the harmonic approximation. By comparing the thermodynamic data, it is indicated that the internal energy and entropy increase, when the mass of the non-metal atoms grows. Fig. 6(b) shows that the contribution to entropy from the non-metal atoms is more important as compared with those from the metal atoms. According to the equation $F = U–TS$, it is obtained that free energy decrease from $LiInS_2$ to $LiInSe_2$ to $LiInTe_2$. At high temperatures the internal energy tends to display k_BT behavior.

In Fig. 6(d and e), we present the results on the temperature dependences of the heat capacity at constant volume (C_V) and Debye temperature Θ_D for the three compounds. In the low-temperature limit, the three C_V exhibit the T^3 power-law behavior, and they all approach at high temperature the classical asymptotic limit of $C_V = 3nk_B = 99.2$ J/(mol K). The heat capacity curves of the three compounds are different at the low-temperature region (<400 K). The heat capacity data increase at the same temperature, when $LiInS_2$ is replaced by $LiInSe_2$ and $LiInSe_2$ is replaced by $LiInTe_2$. At room temperature, the heat capacities are 86.88, 92.30 and 93.89 J/mol K for $LiInS_2$, $LiInSe_2$ and $LiInTe_2$, respectively. The calculated C_V values of three compounds are compared with the experimental C_P values obtained by Yelisseyev and Kuhn [30,31] from Fig. 6(d). Although C_P is different from C_V due to the thermal expansion caused by anharmonicity effects (The relation between C_P and C_V is determined by expression: $C_P - C_V = \alpha_V^2 B_0 VT$, where α_V is the volume thermal expansion coefficient and B_0 is the bulk modulus), the difference is negligible at low temperatures. According to Fig. 6(d) our calculated values of C_V are smaller than the experimental ones of C_P. The temperature dependences of $\Theta_D(T)$ for the three compounds can easily be identified at the whole temperature regions. The Debye temperature increases rapidly below 200 K and reaches a maximum of 520.1, 387.0 and 342.4 K for $LiInS_2$, $LiInSe_2$ and $LiInTe_2$, respectively. Since $\Theta_D(T)$ corresponds to the Debye stiffness, we can reach the conclusion that the Debye stiffness would be enhanced when Te is replaced by Se and Se is replaced by S.

4. Conclusions

We have done a comprehensive ab initio investigations of lattice dynamics and thermodynamic properties of $LiInS_2$, $LiInSe_2$ and $LiInTe_2$ within DFPT frameworks by using quasi-harmonic approximation. The Born effective charges Z^* and high-frequency dielectric tensor ε_∞ indicated the mixed covalent–ionic nature of three compounds. The phonon dispersion curves of three crystals consist of four bands that are observed to be an obvious decrease going from $LiInS_2$ to $LiInSe_2$ to $LiInTe_2$, which is a consequence of the decreasing force constants between cations and anions. The In–X vibrations are mainly located in the lower frequency range and the Li–X vibrations are dominated in the higher frequency range. We have computed the zone-center vibrational frequencies and their eigen displacements and compared the calculated results to the Raman scattering and IR measurements reported in the literature. Our theoretically calculated data are all in good agreement with the available experimental data for these compounds. On going from $LiInS_2$ to $LiInSe_2$ to $LiInTe_2$, the whole lattice vibration spectra move obviously towards the low energy regions. The temperature dependences of the thermodynamic quantities (the internal energy, free energy, heat capacity, entropy and Debye temperature) were calculated. When the mass of the non-metal atoms increase, the internal energy and entropy both increase, while free energy decreases. The results of Debye temperature show that the Debye stiffness would be enhanced when Te is replaced by Se and Se is then replaced by S.

Acknowledgments

This research was supported by the National Natural Science Foundation of China under Projects (No. 50902027) and the Scientific Research Foundation of Mudanjiang Normal University (G201002). The computation resources are provided by the high performance center (HPC) at Harbin Institute of Technology.

References

[1] A. Yelisseyev, A. Titov, K. Lyapunov, V. Drebushchak, L. Isaenko, S. Lobanov, J. Cryst. Growth 275 (2005) e1679–e1684.
[2] L. Isaenko, I. Vasilyeva, A. Yelisseyev, S. Lobanov, V. Malakhov, L. Dovlitova, J.-J. Zondy, I. Kavun, J. Cryst. Growth 218 (2000) 313–322.
[3] L. Isaenko, A. Yelisseyev, S. Lobanov, V. Petrov, F. Rotermund, J.-J. Zondy, G.H.M. Knippels, Mater. Sci. Semicond. Process. 4 (2001) 665–668.
[4] L. Isaenko, A. Yelisseyev, S. Lobanov, P. Krinitsin, V. Petrov, J.-J. Zondy, J. Non-Cryst. Solids 352 (2006) 2439–2443.
[5] L. Isaenko, I. Vasilyeva, A. Merkulov, A. Yelisseyev, S. Lobanov, J. Cryst. Growth 275 (2005) 217–223.
[6] L. Isaenko, I. Vasilyeva, J. Cryst. Growth 310 (2008) 1954–1960.
[7] O. Bidault, S. Fossier, J. Mangin, P. Strimer, A. Yelisseyev, L. Isaenko, S. Lobanov, Solid State Commun. 121 (2002) 207–211.
[8] L. Isaenko, P. Krinitsin, V. Vedenyapin, A. Yelisseyev, A. Merkulov, J.-J. Zondy, V. Petrov, Cryst. Growth Des. 5 (2005) 1325–1329.
[9] V. Petrov, L. Isaenko, A. Yelisseyev, P. Krinitsin, V. Vedenyapin, A. Merkulov, J.-J. Zondy, J. Non-Cryst. Solids 352 (2006) 2434–2438.
[10] T.H. Ma, C.H. Yang, Y. Xie, L. Sun, W.Q. Lv, R. Wang, C.Q. Zhu, M. Wang, Comput. Mater. Sci. 47 (2009) 99–105.
[11] Y.L. Li, W.L. Fan, H.G. Sun, X.F. Cheng, P. Li, X. Zhao, J. Appl. Phys. 106 (2009) 033704–33710.
[12] Yu.M. Basalaev, Yu.N. Zhuravlev, E.B. Kitova, A.S. Poplavnoi, J. Struct. Chem. 48 (2007) 1001–1005.
[13] L.H. Li, J.Q. Li, L.M. Wu, J. Solid State Chem. 181 (2008) 2462–2468.
[14] A.V. Kosobutsky, Yu.M. Basalaev, A.S. Poplavnoi, Phys. Status Solidi B 246 (2009) 364–371.
[15] A.H. Reshak, Physica B 369 (2005) 243–253.
[16] S. Laksari, A. Chahed, N. Abbouni, O. Benhelal, B. Abbar, Mater. Sci. 38 (2006) 223–230.
[17] S. Baroni, S. de Gironcoli, A. dal Corso, P. Giannozzi, Rev. Mod. Phys. 73 (2001) 515–562.
[18] M.D. Segall, P.J.D. Lindan, M.J. Probert, C.J. Pickard, P.J. Hasnip, S.J. Clark, M.C. Payne, J. Phys. Condens. Matter 14 (2002) 2717–2744.
[19] D.R. Hamann, M. Schluter, C. Chiang, Phys. Rev. Lett. 43 (1979) 1494–1497.
[20] J.P. Perdew, A. Zunger, Phys. Rev. B 23 (1981) 5048–5079.
[21] D.M. Ceperley, B.J. Alder, Phys. Rev. Lett. 45 (1980) 566–569.
[22] J.P. Perdew, J.A. Chevary, S.H. Vosko, K.A. Jackson, M.R. Pederson, D.J. Singh, C. Fiolhais, Phys. Rev. B 46 (1992) 6671–6687.
[23] N.W. Ashcroft, N.D. Mermin, Solid State Physics, Saunders College, Philadelphia, 1976.
[24] Ph. Ghosez, J.-P. Michenaud, X. Gonze, Phys. Rev. B 58 (1998) 6224–6240.
[25] T. Kamijoh, T. Nozaki, K. Kuriyama, J. Appl. Phys. 53 (1982) 761–763.
[26] G. Kühn, B. Schumann, D. Oppermann, H. Neumann, H. Sobotta, Z. Anorg. Allg. Chem. 531 (1985) 61–66.
[27] X. Gonze, Phys. Rev. B 55 (1997) 10337–10354.
[28] A. Eifler, V. Riede, J. Bruckner, S. Weise, V. Kramer, G. Lippold, W. Schmitz, K. Bente, W. Grill, Jpn. J. Appl. Phys. 39 (Suppl. 39-1) (2000) 279–281.
[29] E. Gmelin, W. Hönle, Thermochim. Acta 269/270 (1995) 575–590.
[30] G. Kuhn, E. Pirl, H. Neumann, E. Nowak, Cryst. Res. Technol. 22 (1987) 265–269.
[31] A.P. Yelisseyev, V.A. Drebushchak, A.S. Titov, L.I. Isaenko, S.I. Lobanov, K.M. Lyapunov, V.A. Gruzdev, S.G. Komarov, V. Petrov, J.-J. Zondy, J. Appl. Phys. 96 (2004) 3659–3664.